Estimation of Code Ionospheric Biases using Kriging Method

Zhibo Wen*, Yuji Zhu*, Patrick Henkel* and Christoph Günther*,**
*Institute for Communications and Navigation, Technische Universität München
**Institute of Communications and Navigation, German Aerospace Center
zhibo.wen@tum.de, yuji.zhu@tum.de, patrick.henkel@tum.de, christoph.guenther@tum.de

***Abstract*—The code ionospheric bias, also known as the Differential Code Bias (DCB), is an important correction term for single-frequency receiver. This paper proposes a new method to estimate the biases as well as the vertical ionospheric delays using Kriging estimator with a network of receivers. Kriging estimates an unknown variable based on a set of known parameters and a variogram describing the spatial correlation. It is the best estimator in the sense of minimizing the estimation variance. Kriging method is proposed, as it could reconstruct the vertical delays based on a subset to overcome the rank deficiency. A Kalman filter is introduced, and a sub-optimum solution has been obtained based on an iterative Greedy Algorithm. Simulation results have shown cm-level accuracy on the ionospheric bias estimates. The algorithm has also been applied with real GPS data for multiple days, which showed high bias repeatability. The bias estimates have been verified by comparison with published values.**

TABLE OF CONTENTS

1. INTRODUCTION

The GPS code and phase measurements include not only the geometric distance, the clock offsets, the atmospheric delays, etc., but also link-biases which are observed stable over long time [1, 2]. It is thus beneficial to determine the biases and provide them to the user. These link-biases are further assumed to split into receiver- and satellite-dependent parts, e.g. as in [3], which enables the estimation of the biases using a network of receivers [4, 5].

The code biases can be separated into geometric and ionospheric components, where the geometry part goes together with the clock offsets and the ionospheric bias combines with the slant ionospheric delay. The ionospheric bias is seen as the differential group delay between two frequencies, also known as the differential time group delay (TGD) from navigation message [6] or the Differential Code Bias (DCB) from the International GNSS Service (IGS) [7]. A single-frequency receiver must correct this bias, since the satellite clock offset is provided under the ionosphere-free condition.

In order to estimate the ionospheric biases using slant ionospheric delays, the Total Electron Content (TEC) of the ionosphere has to be proper modelled to overcome the rank-deficiency. The ionosphere is typically simplified as a thin shell. Various models have been studied, such as a linear combination of basis functions like bi-cubic splines from Jet Propulsion Laboratory (JPL) [8], or planar fit from Wide Area Augmentation System (WAAS) [9], etc.

Kriging was initially applied in mining and helped estimate the metal concentrations precisely based on sample data. Blanch et al. have first introduced Kriging's method into ionospheric estimation in [10–12]. It takes into account the spatial correlation of the field and provides an optimal solution minimizing the estimation variance. Blanch used Kriging to estimate the ionospheric delay at any ionosphere pierce point after subtracting the satellite and receiver differential biases from the slant delay measurements. He also developed the confidence bound for any given user location.

The method and the challenge in this paper is to estimate the vertical ionospheric delay as well as the differential biases using Kriging. The paper is organized as follows: Section 2 starts from a general model for the GPS measurements, and explains the mapping of the biases. The relationship between the ionospheric biases and the TGDs, DCBs is also presented. The code-aligned phase ionospheric measurement model is explained in Section 3. Section 4 models the variogram, which is important background knowledge for Kriging. The Kriging estimator is introduced in Section 5, while the algorithm combining Kriging with the ionospheric bias estimation is explained in Section 6. Section 7 and 8 show the simulation and real data results, while Section 9 concludes the paper.

2. PARAMETER MAPPING AND SEPARATION OF BIASES

A general model for the code and carrier phase measurements, ρ and $\lambda\varphi$, for receiver i, satellite k on frequency f_m with index $m = 1,\ 2$ is expressed by

$$\begin{aligned}\rho^k_{m,i} &= \left\|\vec{r}_i - \vec{r}^{\,k}\right\| + c(\delta_i - \delta^k) + m^k_{\mathrm{T},i}T_{\mathrm{z},i} + q^2_{1m}I^k_{1,i} + \\ &\quad + b_{m,i} + b^k_m + \eta^k_{m,i}, \\ \lambda_m\varphi^k_{m,i} &= \left\|\vec{r}_i - \vec{r}^{\,k}\right\| + c(\delta_i - \delta^k) + m^k_{\mathrm{T},i}T_{\mathrm{z},i} - q^2_{1m}I^k_{1,i} + \\ &\quad + \lambda_m N^k_{m,i} + \beta_{m,i} + \beta^k_m + \varepsilon^k_{m,i}, \end{aligned} \quad (1)$$

where $\vec{r}_i$ and $\vec{r}^{\,k}$ denote the position vectors of the receiver and the satellite, $c\delta_i$ and $c\delta^k$ denote the receiver and satellite

978-1-4799-5380-6/15/$31.00

clock offsets, $T_{\mathrm{z},i}$ represents the zenith tropospheric delay with $m^k_{\mathrm{T},i}$ the mapping function transforming it into slant delay, $I^k_{1,i}$ is the slant ionospheric delay on the first frequency with the multiplier for different frequency $q^2_{1m} = f^2_1/f^2_m$, λ_m is the wavelength, $N^k_{m,i}$ denotes the integer ambiguity, $\beta_{m,i}$ and β^k_m represent the receiver and satellite phase biases, $b_{m,i}$ and b^k_m are the corresponding code biases, $\varepsilon^k_{m,i}$ and $\eta^k_{m,i}$ represent phase and code noise including multipath. The well-modelled effects including the phase wind-up, the solid earth tides, as well as the prior information on the satellite and receiver phase center offsets and variations, are considered corrected, and thus not appearing in the above model.

The code biases are further separated into geometric and ionospheric components, denoted with indices g and I, i.e.

$$\begin{aligned} b_{m,i} &= b_{\mathrm{g},i} + q^2_{1m} b_{\mathrm{I},i}, \\ b^k_m &= b^k_{\mathrm{g}} + q^2_{1m} b^k_{\mathrm{I}}, \end{aligned} \tag{2}$$

where the code geometric biases are mapped to the clock offsets and the ionospheric biases to the slant delays as

$$\begin{aligned} c\tilde{\delta}_i &= c\delta_i + b_{\mathrm{g},i}, \\ c\tilde{\delta}^k &= c\delta^k - b^k_{\mathrm{g}}, \\ \tilde{I}^k_{1,i} &= I^k_{1,i} + b_{\mathrm{I},i} + b^k_{\mathrm{I}}. \end{aligned} \tag{3}$$

The mapping of the code geometric and ionospheric biases has simplified the code measurement in Eq. (1), and the phase measurement equation should be adapted. Consequently, the code biases are absorbed by the phase biases, i.e.

$$\begin{aligned} \tilde{\beta}_{m,i} &= \beta_{m,i} - b_{\mathrm{g},i} + q^2_{1m} b_{\mathrm{I},i}, \\ \tilde{\beta}^k_m &= \beta^k_m - b^k_{\mathrm{g}} + q^2_{1m} b^k_{\mathrm{I}}. \end{aligned} \tag{4}$$

After the parameter mapping the measurement model turns into

$$\begin{aligned} \rho^k_{m,i} &= \left\|\vec{r}_i - \vec{r}^{\,k}\right\| + c(\tilde{\delta}_i - \tilde{\delta}^k) + m^k_{\mathrm{T},i} T_{\mathrm{z},i} + q^2_{1m} \tilde{I}^k_{1,i} + \eta^k_{m,i} \\ \lambda_m \varphi^k_{m,i} &= \left\|\vec{r}_i - \vec{r}^{\,k}\right\| + c(\tilde{\delta}_i - \tilde{\delta}^k) + m^k_{\mathrm{T},i} T_{\mathrm{z},i} - q^2_{1m} \tilde{I}^k_{1,i} + \\ &\quad + \lambda_m N^k_{m,i} + \tilde{\beta}_{m,i} + \tilde{\beta}^k_m + \varepsilon^k_{m,i}. \end{aligned} \tag{5}$$

The to-be-determined satellite code ionospheric bias b^k_{I} is essentially the same with the differential time group delay defined in the GPS Interface Control Document (ICD) [6]. As described in the ICD, a single-frequency user should correct the satellite clock offset by an additional term, the satellite differential group delay T^k_{GD}. The reason for this is the clock correction coefficient a_{f0} in the navigation message was estimated based on ionosphere-free combination. Thus, the user needs to add the correction term $q^2_{1m} T^k_{\mathrm{GD}}$ onto the code phase measurement $\rho^k_{m,i}$. This shows the consistency in the ionospheric equation in Eq. (3), since the satellite code bias b^k_{I} has also the same frequency coefficient with the ionospheric delay.

The IGS also publishes the receiver and satellite differential code bias estimates to benefit the single-frequency users. The DCB biases are provided in the form of $b_{\mathrm{P1P2}} = b_{\mathrm{P1}} - b_{\mathrm{P2}}$, valid for both receiver and satellite. There exists a linear relationship between the code ionospheric biases $b_{\mathrm{I},i}$, b^k_{I} and the defined receiver and satellite DCB P1P2 biases. Taking the difference between the code biases in Eq. (2) on two frequencies, one obtains

$$\begin{aligned} b_{1,i} - b_{2,i} &= (1 - q^2_{12}) b_{\mathrm{I},i} = b_{\mathrm{P1P2},i}, \\ b^k_1 - b^k_2 &= (1 - q^2_{12}) b^k_{\mathrm{I}} = b^k_{\mathrm{P1P2}}. \end{aligned} \tag{6}$$

A comparison is made between the two bias products from January 2011, i.e. the satellite differential time group delay from navigation message and the differential code bias from IGS. The DCB biases are divided by the coefficient given by Eq. (6) to compare with the time group delays. The difference $T^k_{\mathrm{GD}} - 1/(1 - f^2_1/f^2_2) \cdot b^k_{\mathrm{P1P2}}$ is shown in Fig. 1. A common shift is applied to all satellites in order to align the two products, where the shift is seen as the difference between the references and can be absorbed in the receiver code bias. Therefore, the code ionospheric biases $b_{\mathrm{I},i}$, b^k_{I} which this paper focuses to estimate, have in fact the same meaning of the time group delays and a linear relationship with the differential code biases.

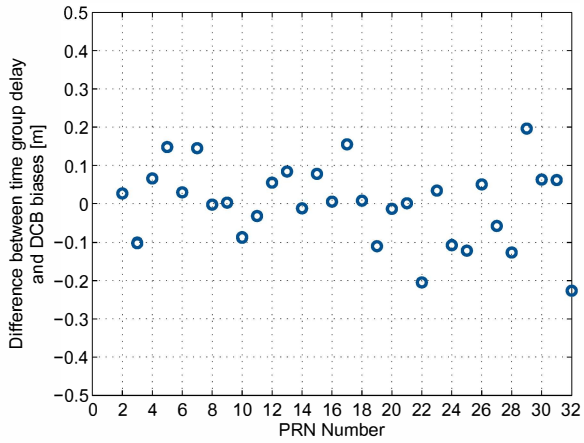

Figure 1. The difference between satellite differential time group delay and the differential code biases in January 2011. PRN 1 was not healthy at that time and has been replaced in GPS week 1645.

3. Ionospheric Measurement Model

To estimate the ionospheric biases, slant ionospheric delays are used as measurements from a network of receivers. There are many possible ways to obtain the slant ionospheric delays. They can come directly from geometry-free ionosphere-preserving code combination, which simultaneously amplifies the noise by over 2 times. Carrier smoothing could be applied afterwards to reduce the noise, however it introduces temporal correlation. Another way could be to augment the code combination with the carrier phase ionosphere-preserving combination, while increasing the unknown parameters by a large number of ambiguities. This could lead to a slow convergence using a network of receivers. In order to avoid adding the ambiguities but to still have low noise, the code-aligned carrier phase combination is employed as suggested by Sardon et al. in [13]. The alignment is done for each receiver-satellite link by determining the constant offset between the code combination and the phase one. In the end, the slant ionospheric delay is obtained as

$$\tilde{\boldsymbol{I}}^k_{1,i} = \boldsymbol{I}^k_{\varphi,i} - \mathcal{E}_t \left[\boldsymbol{I}^k_{\varphi,i} - \boldsymbol{I}^k_{\rho,i} \right], \tag{7}$$

where the vectors $\tilde{\boldsymbol{I}}^k_{1,i}$, $\boldsymbol{I}^k_i$ stack a continuous time series of slant delays on the same measurement link, and the indices φ and ρ denote phase and code combination, respectively.

The ionosphere can be simplified as a single thin layer, which enables us to express the slant delay by the vertical delay $I^k_{1,v,i}$ multiplied with a mapping function $m^k_{\mathrm{I},i}$. Combining with Eq. (3), the ionospheric measurement equation reads

$$\tilde{I}^k_{1,i} = m^k_{\mathrm{I},i} \cdot I^k_{1,v,i} + b_{\mathrm{I},i} + b^k_{\mathrm{I}} + \varepsilon_{I_\varphi}, \tag{8}$$

with the measurement noise being the one of the ionosphere-preserving phase combination. From now on the tilde on the slant delay measurement is dropped for simplicity. The mapping function presents a simple geometry projection, i.e.

$$m^k_{\mathrm{I},i} = \frac{1}{\sqrt{1 - \dfrac{\cos^2 E^k_i}{(1 + h/R_\mathrm{e})^2}}}, \tag{9}$$

with E being the elevation angle, h being the height of the layer, and R_e being the radius of the earth.

It is noticed that, in Eq. (8) the receiver and satellite biases alone form a full-rank system, therefore the biases can only be determined in a relative sense. There are many ways to set the reference. The DCB biases IGS determined are subject to the condition that the sum of the biases is zero [14]. In this paper, we map one reference satellite bias $b^{k'}_{\mathrm{I}}$ into the other satellite biases as $b^k_{\mathrm{I}} - b^{k'}_{\mathrm{I}}$, and compensate it in all receiver biases as $b_{\mathrm{I},i} + b^{k'}_{\mathrm{I}}$.

The fact that the number of slant delays is the same with the number of vertical delays, leaves the system of Eq. (8) still rank-deficient. A proper ionospheric model is expected to further reduce the number of unknown states.

4. Variogram Modelling

In geostatistics, a function $Z(\boldsymbol{x})$ at a given location $\boldsymbol{x}$ depends on some incomplete or unpredictable knowledge, and is thus usually treated as random variable resulting from a random process [15]. Assume a field is intrinsic stationary, for any two nearby locations $\boldsymbol{x}_i$ and $\boldsymbol{x}_j$, we have

$$\begin{aligned} &\mathcal{E}[Z(\boldsymbol{x}_i) - Z(\boldsymbol{x}_j)] = 0, \\ &\mathrm{Var}[Z(\boldsymbol{x}_i) - Z(\boldsymbol{x}_j)] = 2\gamma(\|\boldsymbol{x}_i - \boldsymbol{x}_j\|). \end{aligned} \tag{10}$$

The first property states the random variable $Z(\boldsymbol{x})$ has same mean over a small area, while the second one interprets the difference in variances as a function describing the spatial relation of the field. The function $\gamma(d)$ depends solely on the relative distance d rather than the absolute locations, and is known as the semi-variogram. The term "semi" is used because γ is one half of the variance in Eq. (10). To clarify, this term is omitted for simplicity and γ is called variogram in this paper.

Given a set of sample data measured at known locations, an empirical variogram can be calculated as

$$\gamma(d) = \frac{1}{2m(d)} \sum_{\|\boldsymbol{x}_i - \boldsymbol{x}_j\| \in [d - \frac{1}{2}\Delta d, d + \frac{1}{2}\Delta d]} (Z(\boldsymbol{x}_i) - Z(\boldsymbol{x}_j))^2, \tag{11}$$

where $m(d)$ denotes the number of pairs whose distances fall into the range of $[d - \frac{1}{2}\Delta d, d + \frac{1}{2}\Delta d]$.

A set of vertical ionospheric delays are collected from the IGS final TEC grid product during the night on Jan. 1, 2011. Moreover, the vertical delays have subtracted a mean vertical TEC map obtained by averaging the TEC maps over sun-synchronous same geomagnetic locations over 8 years, so that the residual field can be assumed to meet the requirement of intrinsic stationary. The random variable $Z(\boldsymbol{x})$ is thus defined as suggested in [3] as

$$Z(\boldsymbol{x}) = I_v(\boldsymbol{x}) - \mathcal{E}_t[I_v(\boldsymbol{x})]. \tag{12}$$

Fig. 2 shows an example of empirical variogram in blue dots. The region of interest lies in latitude between $30°$ and $87.5°$, and longitude between $-30°$ and $75°$. The distance interval Δd is set to 50 km. The variogram increases as the distance between pairs of points grows, and becomes saturated when the distance is larger than a certain threshold, e.g. 4000 km in the plot.

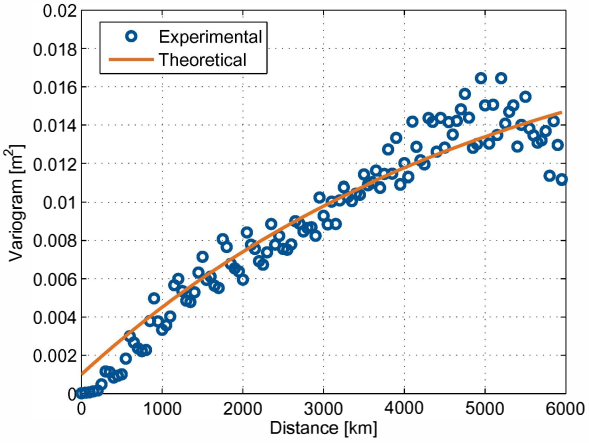

Figure 2. The calculated experimental and fitted exponential variograms in the night for the region of latitude from $30°$ to $87.5°$ and longitude from $-30°$ to $75°$. As the distance increases, the variogram first increases almost linearly and then tends to converge at large distances.

As the empirical variogram is a discrete function, we would need to fit it to a continuous one to represent the spatial relation of any distance. In this paper we have applied a much used negative exponential function, suggested in [15, 16], i.e.

$$\gamma(d) = c_0(1 - e^{-d/a_0}) + c_n. \tag{13}$$

The function has the value c_n when the distance is zero, and approaches a sill $c_0 + c_n$ when the distance goes to infinity. The variable a_0 defines the spatial extent of the model. The fitted theoretical model is shown in orange in Fig. 2, with the parameters chosen as $c_0 = 0.001$ m^2, $c_n = 0.02$ m^2, and $a_0 = 5176.5$ km.

5. Fundamentals of Ordinary Kriging

Kriging is a widely used method in geostatistics, to estimate the value at a given point based on some existing samples at known points and a certain prior knowledge on the spatial variation. The most robust and most used method among

many is ordinary Kriging [15]. Consider a random variable $Z(\boldsymbol{x}_0)$ at location $\boldsymbol{x}_0$, its estimate is expressed by a linear combination of the existing data with different weights, i.e.

$$\hat{Z}(\boldsymbol{x}_0) = \sum_{i=1}^{n} \alpha_i Z(\boldsymbol{x}_i), \quad \text{s.t.} \quad \sum_{i=1}^{n} \alpha_i = 1. \tag{14}$$

The estimate is unbiased due to the condition that the sum of the weight is one. This can be straightforward verified through the mean equality property in Eq. (10). The variance of the estimation error is given in [15] as

$$\begin{aligned} &\mathrm{Var}[\hat{Z}(\boldsymbol{x}_0) - Z(\boldsymbol{x}_0)] \\ &= 2\sum_{i=1}^{n} \alpha_i \gamma(\|\boldsymbol{x}_0 - \boldsymbol{x}_i\|) - \sum_{i=1}^{n}\sum_{j=1}^{n} \alpha_i \alpha_j \gamma(\|\boldsymbol{x}_i - \boldsymbol{x}_j\|) \\ &= 2\boldsymbol{A}^{\mathrm{T}}\boldsymbol{\Gamma} - \boldsymbol{A}^{\mathrm{T}}\boldsymbol{G}\boldsymbol{A}, \end{aligned} \tag{15}$$

with the matrices denoting

$$\begin{aligned} \boldsymbol{A} &= \begin{bmatrix} \alpha_1 \\ \vdots \\ \alpha_n \end{bmatrix}, \boldsymbol{\Gamma} = \begin{bmatrix} \gamma(\|\boldsymbol{x}_0 - \boldsymbol{x}_1\|) \\ \vdots \\ \gamma(\|\boldsymbol{x}_0 - \boldsymbol{x}_n\|) \end{bmatrix}, \\ \boldsymbol{G} &= \begin{bmatrix} \gamma(\|\boldsymbol{x}_1 - \boldsymbol{x}_1\|) & \dots & \gamma(\|\boldsymbol{x}_1 - \boldsymbol{x}_n\|) \\ \vdots & \ddots & \vdots \\ \gamma(\|\boldsymbol{x}_n - \boldsymbol{x}_1\|) & \dots & \gamma(\|\boldsymbol{x}_n - \boldsymbol{x}_n\|) \end{bmatrix}. \end{aligned} \tag{16}$$

Kriging provides the best solution for $\boldsymbol{A}$ in the sense that the variance of the estimation error in Eq. (15) is minimized under the constraint in Eq. (14). A Lagrange multiplier μ is introduced to solve the minimization, which yields

$$\hat{\tilde{\boldsymbol{A}}} \triangleq \begin{bmatrix} \hat{\boldsymbol{A}} \\ \hat{\mu} \end{bmatrix} = \begin{bmatrix} \boldsymbol{G} & \boldsymbol{1} \\ \boldsymbol{1}^{\mathrm{T}} & \boldsymbol{0} \end{bmatrix}^{-1} \cdot \begin{bmatrix} \boldsymbol{\Gamma} \\ 1 \end{bmatrix} \triangleq \tilde{\boldsymbol{G}}^{-1}\tilde{\boldsymbol{\Gamma}}. \tag{17}$$

The estimation variance on the $\hat{Z}(\boldsymbol{x}_0)$ estimate is further obtained as

$$\mathrm{Var}[\hat{Z}(\boldsymbol{x}_0) - Z(\boldsymbol{x}_0)] = \tilde{\boldsymbol{\Gamma}}^{\mathrm{T}}\tilde{\boldsymbol{G}}^{-1}\tilde{\boldsymbol{\Gamma}}. \tag{18}$$

Eq. (17) and (18) are the solutions from the Kriging estimator, which is a best linear unbiased estimator. The weighting coefficients depend on the spatial relation between the studied point and the sample points, where the variogram describes the spatial information and is needed a priori. As a result of Eq. (17) and the variogram function, the points which are nearer the studied point would have a larger weight and thus contribute more in the interpolation, while the points farther away have less impact.

6. METHODOLOGY

Kriging provides an optimal way of representing a subset of sample points by another subset, which enables us to overcome the rank-deficiency in Eq. (8). Let us consider a network of R receivers with totally K satellites in view, while receiver i sees K_i satellites. The number of receiver and satellite biases is $R + K - 1$ in total. As pointed out in Section 3, there are at least $R + K - 1$ ionospheric vertical delays that have to be mapped. These mapped vertical delay parameters do not appear in the state vector, instead they are interpolated with Kriging using the subset to be estimated.

A Kalman filter is introduced to estimate the subset of vertical delays and the ionospheric biases. We denote the estimated subset by an upper index s, and the other subset of vertical delays to be interpolated by $\bar{\mathrm{s}}$. The measurement model in Eq. (8) can be rewritten in matrix-vector form as

$$\boldsymbol{I} = \left[\boldsymbol{H}_{I_{\mathrm{v}}}, \boldsymbol{H}_{b_{\mathrm{I,rec}}}, \boldsymbol{H}_{b_{\mathrm{I}}^{\mathrm{sat}}}\right] \cdot \begin{bmatrix} \boldsymbol{I}_{\mathrm{v}}^{\mathrm{s}} \\ \boldsymbol{b}_{\mathrm{I,rec}} \\ \boldsymbol{b}_{\mathrm{I}}^{\mathrm{sat}} \end{bmatrix} + \boldsymbol{\varepsilon}_I, \tag{19}$$

where the vectors are given as

$$\begin{aligned} \boldsymbol{I} &= \left[I_{1,1}^{1}, \dots, I_{1,1}^{K_1}, \dots, I_{1,R}^{1}, \dots, I_{1,R}^{K_R}\right]^{\mathrm{T}}, \\ \boldsymbol{I}_{\mathrm{v}} &= \left[I_{1,v,1}^{1}, \dots, I_{1,v,1}^{K_1}, \dots, I_{1,v,R}^{1}, \dots, I_{1,v,R}^{K_R}\right]^{\mathrm{T}}, \\ \boldsymbol{b}_{\mathrm{I,rec}} &= \left[b_{\mathrm{I},1}, b_{\mathrm{I},2}, \dots, b_{\mathrm{I},R}\right]^{\mathrm{T}}, \\ \boldsymbol{b}_{\mathrm{I}}^{\mathrm{sat}} &= \left[b_{\mathrm{I}}^{1}, \dots, b_{\mathrm{I}}^{k'-1}, b_{\mathrm{I}}^{k'+1}, \dots, b_{\mathrm{I}}^{K}\right]^{\mathrm{T}}, \end{aligned} \tag{20}$$

with k' being the reference satellite. The design matrix for vertical delays contains two parts, the mapping functions alone and and the functions multiplied with the Kriging coefficients, i.e.

$$\boldsymbol{H}_{I_{\mathrm{v}}} = \begin{bmatrix} m_{\mathrm{I},1}^{\bar{\mathrm{s}}}\alpha_{1,1} & \dots & \dots & \dots & m_{\mathrm{I},1}^{\bar{\mathrm{s}}}\alpha_{1,n_{\mathrm{s}}} \\ m_{\mathrm{I},1}^{\mathrm{s}} & 0 & \dots & \dots & 0 \\ \vdots & \vdots & \vdots & \vdots & \vdots \\ m_{\mathrm{I},j}^{\bar{\mathrm{s}}}\alpha_{j,1} & \dots & \dots & \dots & m_{\mathrm{I},j}^{\bar{\mathrm{s}}}\alpha_{j,n_{\mathrm{s}}}, \\ 0 & \dots & m_{\mathrm{I},i}^{\mathrm{s}} & \dots & 0 \\ \vdots & \vdots & \vdots & \vdots & \vdots \\ m_{\mathrm{I},n_{\bar{\mathrm{s}}}}^{\bar{\mathrm{s}}}\alpha_{n_{\bar{\mathrm{s}}},1} & \dots & \dots & \dots & m_{\mathrm{I},n_{\bar{\mathrm{s}}}}^{\bar{\mathrm{s}}}\alpha_{n_{\bar{\mathrm{s}}},n_{\mathrm{s}}} \end{bmatrix}, \tag{21}$$

with n_s and $n_{\bar{s}}$ being the number of pierce points in the estimated subset $\boldsymbol{S}$ and the mapped (complement) subset $\bar{\boldsymbol{S}}$ respectively. For each pierce point j belonging to the mapped subset, the vertical delay is interpreted with a linear combination of the estimated subset of vertical delays. The weighting coefficients are determined by Kriging method and are combined in the vector $\boldsymbol{\alpha}_j$ as

$$\boldsymbol{\alpha}_j = [\alpha_{j,1}, \alpha_{j,2}, \dots, \alpha_{j,n_s}]^{\mathrm{T}}, \text{ with } j \in \{1, \dots, n_{\bar{\mathrm{s}}}\}. \tag{22}$$

If we rearrange the measurements in two categories, the Kriging solution in Eq. (17) can be built in Eq. (21), and a permutation matrix $\boldsymbol{P}$ can be introduced to restore the measurement ordering, i.e.

$$\begin{aligned} \boldsymbol{H}_{I_{\mathrm{v}}} &= \boldsymbol{P} \cdot \begin{bmatrix} \mathrm{diag}(\boldsymbol{m}_{\mathrm{I}}^{\mathrm{s}}) \\ \mathrm{diag}(\boldsymbol{m}_{\mathrm{I}}^{\bar{\mathrm{s}}}) \cdot \begin{bmatrix} \boldsymbol{\alpha}_1^{\mathrm{T}} \\ \vdots \\ \boldsymbol{\alpha}_{n_{\bar{\mathrm{s}}}}^{\mathrm{T}} \end{bmatrix} \end{bmatrix} \\ &= \boldsymbol{P} \cdot \begin{bmatrix} \mathrm{diag}(\boldsymbol{m}_{\mathrm{I}}^{\mathrm{s}}) \\ \mathrm{diag}(\boldsymbol{m}_{\mathrm{I}}^{\bar{\mathrm{s}}}) \cdot \begin{bmatrix} (\boldsymbol{D} \cdot (\tilde{\boldsymbol{G}}^{\mathrm{s}})^{-1}\tilde{\boldsymbol{\Gamma}}_1)^{\mathrm{T}} \\ \vdots \\ (\boldsymbol{D} \cdot (\tilde{\boldsymbol{G}}^{\mathrm{s}})^{-1}\tilde{\boldsymbol{\Gamma}}_{n_{\bar{\mathrm{s}}}})^{\mathrm{T}} \end{bmatrix} \end{bmatrix}, \end{aligned} \tag{23}$$

with $\tilde{\boldsymbol{G}}^{\mathrm{s}}$ and $\tilde{\boldsymbol{\Gamma}}_j$ ($j \in \{1, \dots, n_{\bar{\mathrm{s}}}\}$) following the definition in

Eq. (17), and $\boldsymbol{D}$ being the selection matrix as

$$\tilde{\boldsymbol{G}}^{\mathrm{s}} = \begin{bmatrix} \gamma(\|\boldsymbol{x}_1^{\mathrm{s}} - \boldsymbol{x}_1^{\mathrm{s}}\|) & \dots & \gamma(\|\boldsymbol{x}_1^{\mathrm{s}} - \boldsymbol{x}_{n_{\mathrm{s}}}^{\mathrm{s}}\|) & 1 \\ \vdots & \ddots & \vdots & \vdots \\ \gamma(\|\boldsymbol{x}_{n_{\mathrm{s}}}^{\mathrm{s}} - \boldsymbol{x}_1^{\mathrm{s}}\|) & \dots & \gamma(\|\boldsymbol{x}_{n_{\mathrm{s}}}^{\mathrm{s}} - \boldsymbol{x}_{n_{\mathrm{s}}}^{\mathrm{s}}\|) & 1 \\ 1 & \dots & 1 & 0 \end{bmatrix},$$

$$\tilde{\boldsymbol{\Gamma}}_j = \begin{bmatrix} \gamma(\|\boldsymbol{x}_j^{\bar{\mathrm{s}}} - \boldsymbol{x}_1^{\mathrm{s}}\|) \\ \vdots \\ \gamma(\|\boldsymbol{x}_j^{\bar{\mathrm{s}}} - \boldsymbol{x}_{n_{\mathrm{s}}}^{\mathrm{s}}\|) \end{bmatrix}, \boldsymbol{D} = \left[\mathbf{I}^{n_{\mathrm{s}} \times n_{\mathrm{s}}}, \mathbf{0}^{n_{\mathrm{s}} \times 1}\right] \tag{24}$$

The design matrix for the receiver biases is given as

$$\boldsymbol{H}_{b_{\mathrm{I,rec}}} = \begin{bmatrix} \mathbf{1}^{K_1 \times 1} & & & \\ & \mathbf{1}^{K_2 \times 1} & & \\ & & \ddots & \\ & & & \mathbf{1}^{K_R \times 1} \end{bmatrix}, \tag{25}$$

and for the satellite biases as

$$\boldsymbol{H}_{b_{\mathrm{I}}^{\mathrm{sat}}} = \begin{bmatrix} \boldsymbol{H}_{b_{\mathrm{I}}^{K_1}} \\ \vdots \\ \boldsymbol{H}_{b_{\mathrm{I}}^{K_R}} \end{bmatrix}, \tag{26}$$

where each component $\boldsymbol{H}_{b_{\mathrm{I}}^{K_i}}$ has the dimension $K_i \times (K-1)$. For the j-th row in $\boldsymbol{H}_{b_{\mathrm{I}}^{K_i}}$, only the k_{ij}-th column has the entry 1 while the other columns have 0s. k_{ij} is defined as the index of the j-th ($j = 1, \dots, K_i$) visible satellite from receiver i in the total visible $K-1$ satellites (excluded the reference satellite). If the j-th satellite happens to be the reference satellite, no index can be found in the $K-1$ satellites, thus the j-th row in $\boldsymbol{H}_{b_{\mathrm{I}}^{K_i}}$ is an all-zero row.

After representing the mapped subset with the estimated one, the measurement noise shall be adjusted accordingly. The new measurement noise for the mapped subset should contain not only the noise from the slant delay measurements, but also the Kriging estimation error.

Until this stage, a full-rank ionospheric measurement model has been established by mapping a subset of vertical delays with Kriging. However, how to construct the mapped subset still remains an open question. The question includes how many vertical delays and which ones should be mapped away. Intuitively the more pierce points stay in the estimated subset, the better the interpolation would be. However, the improvement of the interpolation would be little when sufficient vertical delays have already been included in the state vector. The convergence of the estimation would also be slower in general if there are more unknowns. Least-squares method could be applied to Eq. (19) for a global optimal solution, whereas the coefficient matrices $\boldsymbol{H}_{I_{\mathrm{v}}}$ as well as $\boldsymbol{H}_{b_{\mathrm{I,rec}}}$ and $\boldsymbol{H}_{b_{\mathrm{I}}^{\mathrm{sat}}}$ need to be fixed. However, they depend on a specific choice of estimated vertical delay subset. A brute-force search would find the minimum by examining all possible subsets. This would however be inefficient and even infeasible for a typical scenario of hundreds to thousands of ionospheric pierce points.

We propose an efficient Greedy algorithm to obtain a sub-optimum solution for Eq. (19), which constructs the estimated subset of vertical delays in an iterative manner. The initialization of the subset starts with the first point selected geographically about in the middle of the map,

$$\hat{\boldsymbol{x}}_1 = \arg\min_{\boldsymbol{x}_1}(|\phi(\boldsymbol{x}_1) - \bar{\phi}| + |\lambda(\boldsymbol{x}_1) - \bar{\lambda}|), \tag{27}$$

so that the distances and the spatial relations to other points are averaged. The variables ϕ and λ denote the latitude and longitude of a pierce point respectively, while $\bar{\phi}$ and $\bar{\lambda}$ are the average latitude and longitude for the region of interest. Then all other points are represented by the first one using Kriging interpolation, consequently they will all have a weighting coefficient 1 but different variances. The second point included should have the least accurately determined vertical delay. Thus it is chosen as the farthest point to the first one, because the variogram is the largest. At the next step, each remaining point is calculated based on the interpolation between the two points in the estimated subset. Thus the subsequent point is always chosen as the one having the largest Kriging variance based on the already selected points, i.e.

$$\hat{\boldsymbol{x}}_i = \arg\max_{\boldsymbol{x}_i} \left\{ \mathrm{Var}\left[\hat{Z}(\boldsymbol{x}_i) - Z(\boldsymbol{x}_i)\right] \right\} \tag{28}$$

with the estimate

$$\hat{Z}(\boldsymbol{x}_i) = \sum_{j=1}^{i-1} \lambda_j Z(\boldsymbol{x}_j), \quad i > 1.$$

The selection procedure stops until the Kriging variances on the remaining points are below a certain threshold, which means the selected points can well generate the others.

Furthermore, the pierce points would change their positions as the satellite geometry changes, and they would even be removed when the satellite is no longer visible. Therefore the subset points need to be updated and reselected during the estimation, since better subset choice would come up as relative positions of pierce points change over time. If a new point is included in the subset, its vertical delay estimate needs to be introduced to the state vector of the Kalman filter, so do the variance and covariance with other vertical delays. The vertical delay at the new subset point is initialized as the interpolated value based on the previous subset used for Kriging

$$\hat{I}_{\mathrm{v},\bar{s}_j}^{\tilde{\mathrm{s}},-}(t) = \boldsymbol{\alpha}_j^{\mathrm{T}} \cdot \hat{\boldsymbol{I}}_{\mathrm{v}}^{\mathrm{s},+}(t-1), \tag{29}$$

where the new point $\bar{s}_j$ belonged to the mapped subset at epoch $t-1$. Assume the previous estimated subset contains pierce points $\boldsymbol{S} = \{s_1, \dots, s_{n_{\mathrm{s}}}\}$, then the new estimated subset is $\tilde{\boldsymbol{S}} = \{s_1, \dots, s_{n_{\boldsymbol{s}}}, \bar{s}_j\}$. At epoch t, the a priori covariance matrix $\hat{\boldsymbol{P}}$ is calculated as

$$\hat{\boldsymbol{P}}_{\tilde{\boldsymbol{S}}\tilde{\boldsymbol{S}}}^{-}(t) = \begin{bmatrix} \hat{\boldsymbol{P}}_{\boldsymbol{S}\boldsymbol{S}}^{-}(t) & \hat{\boldsymbol{P}}_{\boldsymbol{S}\bar{s}_j}^{-}(t) \\ \hat{\boldsymbol{P}}_{\bar{s}_j\boldsymbol{S}}^{-}(t) & \hat{\boldsymbol{P}}_{\bar{s}_j\bar{s}_j}^{-}(t) \end{bmatrix}, \tag{30}$$

where the upper left element comes from the prediction step of Kalman filtering, and the other three terms need to be initialized. The variance of the new vertical delay estimate is obtained from Kriging estimation variance as

$$\begin{aligned} \hat{\boldsymbol{P}}_{\bar{s}_j\bar{s}_j}^{-}(t) &= \mathcal{E}\left[\left(\hat{I}_{\mathrm{v},\bar{s}_j}^{\tilde{\mathrm{s}},-}(t) - I_{\mathrm{v},\bar{s}_j}^{\tilde{\mathrm{s}},-}(t)\right)^2\right] \\ &= \boldsymbol{\alpha}_j^{\mathrm{T}} \hat{\boldsymbol{P}}_{\boldsymbol{S}\boldsymbol{S}}^{+}(t-1)\boldsymbol{\alpha}_j. \end{aligned} \tag{31}$$

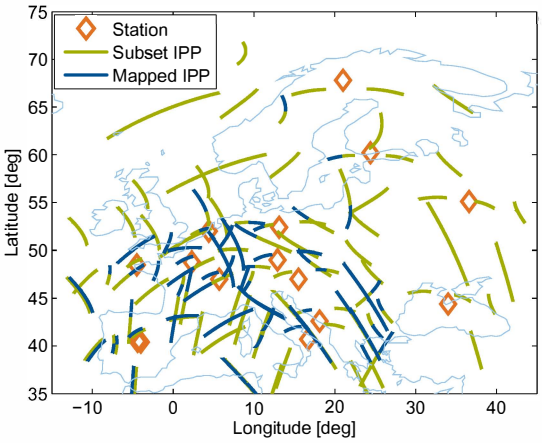

Figure 3. The 15 IGS Stations (as orange diamonds) and the trajectories of the ionospheric pierce points. The estimated vertical delays are shown in green, whereas the mapped pierce points are in blue. Most of the points at the edges of the map are selected into the estimated subset, except those which are near the subset points.

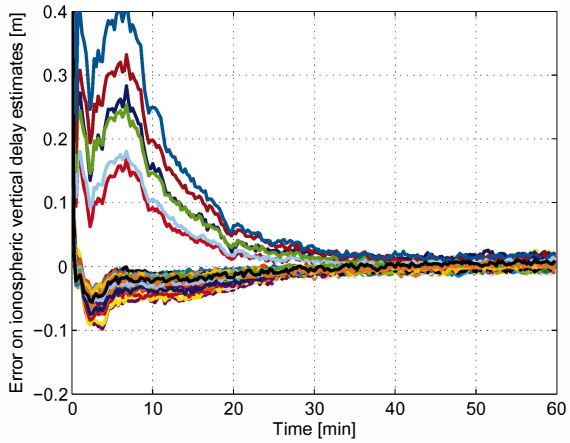

Figure 4. Error on the ionospheric subset vertical delay estimates. Each line represents one vertical delay at a pierce point. The errors have converged to under 2 cm.

The off-diagonal terms in Eq. (30) are calculated as

$$\hat{\boldsymbol{P}}^{-}_{\boldsymbol{S}\bar{s}_j}(t) = \left(\hat{\boldsymbol{P}}^{-}_{\bar{s}_j\boldsymbol{S}}(t)\right)^{\mathrm{T}} = \hat{\boldsymbol{P}}^{+}_{\boldsymbol{SS}}(t-1)\boldsymbol{\alpha}_j \qquad (32)$$

7. Simulation Results

The suggested algorithm has been tested first with a simulation to estimate the vertical ionospheric delays and the biases. The simulation takes 15 IGS stations in the region of Europe, shown as orange diamond symbols in Fig. 3. The time period is chosen from 20:00 to 21:00 on Jan. 1, 2011. We use the negative exponential function calculated in Section 4 for the theoretical variogram.

In order to keep the simulation simple, no rising or setting satellite is considered, i.e. only the satellites which are always visible are counted. Moreover, the satellites which are visible to less than 4 stations are also ruled out, so that the satellite biases could converge well. There are in total 112 pierce points, of which 70 points are selected into the subset and their vertical delays are directly estimated. The other 42 points are interpolated as linear combinations of the subset points, with coefficients determined optimally with Kriging.

The measurement noise is set to 2 cm for the slant ionospheric delays, while the process noise in the Kalman filter is configured as 0.5 cm for the vertical delays, and 1 mm for the satellite and receiver ionospheric biases.

A subset reselection is performed at the 30th minute, while the trajectories of the changed points are shown with half green and half blue in Fig. 3. The impacts on the estimation of the vertical delays, as well as of the receiver and satellite biases, are shown in Fig. 4 and Fig. 5.

In Fig. 4, the errors on the vertical delays are converged under 10 cm after 18 minutes and drop further to under 2 cm. After replacing with a new optimal subset at epoch 1800, the accuracy of the vertical delays remain under 2 cm. In Fig. 5, the benefit of changing the subset is seen after 30 minutes, which results in an accuracy of below 2 cm. Also, one observes in Fig. 5 that the satellite biases are estimated more accurately than the receiver ones, as each satellite is seen by about 15 receivers and each receiver only sees about 7 satellites in the simulation.

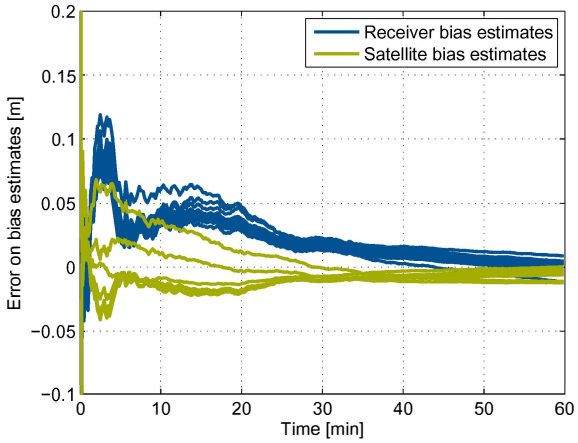

Figure 5. Error on the satellite and receiver ionospheric bias estimates. A change of the subset at 30 minute fastens the convergence of the bias estimates. In addition, a slightly better accuracy can be observed at the satellite bias estimates than the receiver ones, because of more measurements for each satellite.

8. Real Data Analysis

We have also applied the estimation algorithm with real GPS data from a larger network including 24 IGS stations. The GPS code and phase measurements on two frequencies were collected from Jan. 1 to Jan. 14, 2011, with 6 hours during the night each day for the consecutive two weeks. The data period is from 20:00 to 02:00 UTC. The slant delays come from the code-aligned phase ionosphere-free combination. We've subtracted a mean vertical delay map averaged at sun-synchronous same geomagnetic locations from 2003 to 2010.

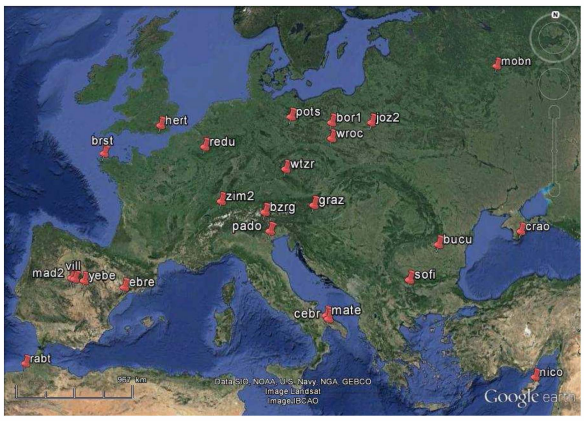

Figure 6. Network of the 24 IGS stations, shown in red pins.

The residuals from all stations are plotted in Fig. 7. The blue histogram indicates the estimation using Kriging and the iterative Greedy algorithm, while the black one shows the residuals when subtracting the IGS ionospheric grid map and the differential code biases from the measurements. The residuals from the Kriging method approach zero-mean and a standard deviation of $0.2\mathrm{m}$, which is much smaller than the sigma in the case of subtracting IGS products. It should be fairly pointed out that the IGS products are estimated with several hundred stations among different analysis centers [17], and thus the residuals are averaged in a global sense, whereas in our case a regional network is being studied.

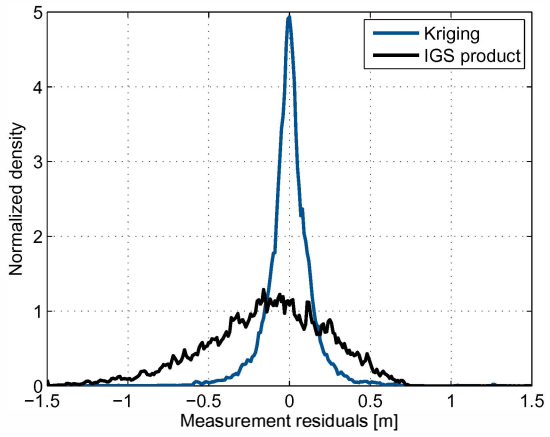

Figure 7. Comparison of the estimation residuals for all stations on Jan. 1 2011. The residuals from the Kriging method are unbiased and concentrate highly around zero while the one from subtracting IGS products results in a bias of -0.2 m and a larger variance.

Fig. 8 depicts the estimated satellite biases over 2 weeks. A high repeatability is observed on each bias estimate, with the most stable one varying about 6 cm over 14 days.

We would also like to compare the bias estimates with the IGS differential code biases, in order to validate the correctness of the biases. Since the IGS satellite DCBs are subject to the zero-sum condition and our estimates have been absorbed the bias from one reference satellite, the two bias products are first aligned. Therefore, for all the satellites between the two products we determine a common offset, which is assigned as the bias value for the reference satellite to meet the zero-sum

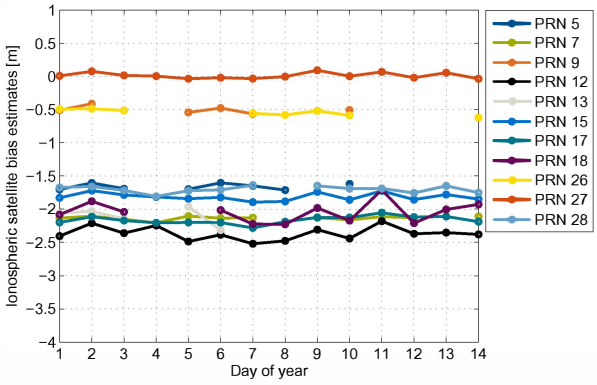

Figure 8. The satellite code bias estimates projected into the ionosphere show a very high repeatability over 2 weeks. The smallest variation is seen on the bias estimate from PRN 9 with about 6 cm over 14 days.

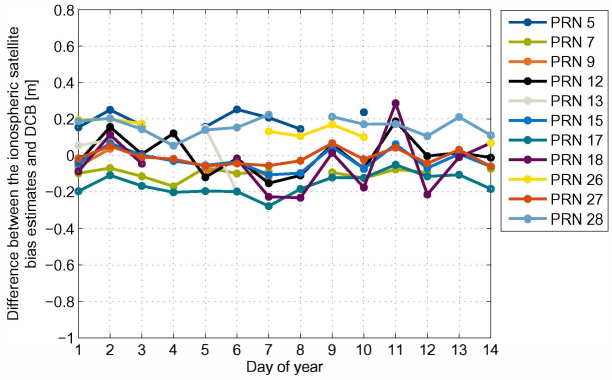

Figure 9. Difference between the satellite ionospheric biases and the IGS differential code biases over 2 weeks.

condition. Fig. 9 shows the difference over the consecutive 14 days. Most of the differences on the bias estimates are under 20 cm.

9. Conclusions

In this paper we have proposed a new ionospheric estimation method, which represents a subset of vertical delays with the remaining ones. The key to a successful representation is a minimum loss of information, which is made possible by the best linear unbiased Kriging estimator. It exploits the spatial correlation of the ionosphere through the variogram. The simulation and real data results have shown accurate vertical delay and bias estimates, while the comparison to the IGS differential code biases confirms the correctness of our bias estimates.

It should be mentioned that the experiment data was selected in the night when the ionosphere is quiet. However the algorithm always estimates a subset of vertical delays which relate directly to the instant measurements. Thus it is reasonable to expect a similar accuracy during the daytime, as long as the variogram could well describe the field. Moreover, the more precise corrections of the vertical delays and the biases obtained from the Kriging algorithm could enable a single-frequency receiver to position itself with better accuracy.

REFERENCES

[1] E. Sardon and N. Zarraoa, "Estimation of the total electron content using GPS data: How stable are the differential satellite and receiver instrumental biases?" *Radio Science*, vol. 32, no. 5, pp. 1899–1910, 1997.

[2] M. Ge, G. Gendt, M. Rothacher, C. Shi, and J. Liu, "Resolution of GPS carrier-phase ambiguities in precise point positioning (PPP) with daily observations," *Journal of Geodesy*, vol. 82, no. 7, pp. 389–399, 2008.

[3] C. Günther, *Lecture notes on satellite navigation*. Technische Universität München, 2013.

[4] P. Henkel, Z. Wen, and C. Günther, "Estimation of code and phase biases on multiple frequencies with a kalman filter," in *Proceedings of the 4th European Workshop on GNSS Signals and Signal Processing*, 2009.

[5] Z. Wen, P. Henkel, and C. Günther, "Reliable estimation of phase biases of GPS satellites with a local reference network," in *Proceedings of 53rd IEEE Intl Symp ELMAR*. IEEE, 2011, pp. 321–324.

[6] Navstar, "Navstar GPS Space Segment/Navigation User Interfaces," *Arinc research corporation*, 2000.

[7] J. Kouba, "A guide to using International GNSS Service (IGS) products," *International GNSS*, 2009.

[8] A. Mannucci, B. Wilson, D. Yuan, C. Ho, U. Lindqwister, and T. Runge, "A global mapping technique for gps-derived ionospheric total electron content measurements," *Radio science*, vol. 33, no. 3, pp. 565–582, 1998.

[9] A. Komjathy, L. Sparks, A. J. Mannucci, and X. P. Nasa, "An assessment of the current waas ionospheric correction algorithm in the south american region," *Navigation(Washington)*, vol. 50, no. 3, pp. 193–204, 2003.

[10] J. Blanch, "An ionosphere estimation algorithm for WAAS based on Kriging," in *Proceedings of ION GPS*, 2002, pp. 24–27.

[11] J. Blanch, T. Walter, and P. Enge, "Application of spatial statistics to ionosphere estimation for WAAS," in *Proceedings of ION NTM*, vol. 10, 2002, pp. 24–40.

[12] ——, "Adapting Kriging to the WAAS MOPS ionospheric grid," in *Proceedings of ION NTM*, 2003.

[13] E. Sardon, A. Rius, and N. Zarraoa, "Estimation of the transmitter and receiver differential biases and the ionospheric total electron content from Global Positioning System observations," *Radio Science*, vol. 29, no. 3, pp. 577–586, 1994.

[14] J. Feltens, "IGS ionosphere models comparison," in *IGS Presentation, JPL Ionosphere Workshop*, 1998.

[15] R. Webster and M. A. Oliver, *Geostatistics for environmental scientists*. John Wiley & Sons, 2007.

[16] J. Blanch, "Using Kriging to bound satellite ranging errors due to the ionosphere," Ph.D. dissertation, Stanford University, 2003.

[17] A. Krankowski and M. Hernandez-Pajares, "Status of the IGS ionosphere products and future developments," in *IGS Analysis Center Workshop*, 2008.

BIOGRAPHY

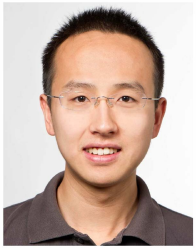

Zhibo Wen *received his Bachelor and Master degree passed with high distinction in Electrical Engineering and Information Technology, from Shanghai Jiao Tong University in 2008 and from Technische Universität München in 2010 respectively. He is currently a PhD candidate at the Institute for Communications and Navigation at Technische Universität München. His research interests include precise point positioning, estimation and validation of satellite and receiver biases.*

Yuji Zhu *received her Bachelor and Master degree in Electrical Engineering from Shanghai Jiao Tong University in 2009, and from Technische Universität München in 2014, respectively. She has been working on the topic of ionospheric bias estimation for her master thesis at the Institute for Communications and Navigation at Technische Universität München.*

Patrick Henkel *has received his Bachelor, Master and PhD with summa cum laude from the Technische Universität München, Germany. He is currently working on his habilitation on precise point positioning at TUM. He had received the Pierre Contensou Gold Medal in 2007, the 1st prize in Bavaria at the European Satellite Navigation Competition in 2010 and a dissertation award of the Vodafone Research Foundation for his PhD thesis in 2011.*

Christoph Günther *studied theoretical physics at the Swiss Federal Institute of Technology in Zurich. He received his diploma in 1979 and completed his PhD in 1984. He worked on communication and information theory at Brown Boveri and Ascom Tech. From 1995, he led the development of mobile phones for GSM and later dual mode GSM/Satellite phones at Ascom. In 1999, he became head of the research department of Ericsson in Nuremberg. Since 2003, he is the director of the Institute of Communication and Navigation at the German Aerospace Center (DLR) and since December 2004, he additionally holds a Chair at the Technische Universität München (TUM). His research interests are in satellite navigation, communication and signal processing.*